Enhanced NIR emission in Ce^{3+}/Er^{3+}-doped YAG induced by Bi^{3+} doping

Xiaohai Liu (刘小海)[1], Siguo Xiao (肖思国)[1*], Zhifeng Xiang (向志锋)[1], Biyao Zhou (周碧遥)[1], Qing Wen (文 晴)[1], Xiaoliang Yang (阳效良)[1], and Xiangliang Jin (金湘亮)[2]

[1]*Faculty of Materials, Optoelectronics and Physics, Institute for Nanophysics and Rare-earth Luminescence, Xiangtan University, Xiangtan 411105, China*

[2]*Faculty of Materials, Optoelectronics and Physics, Xiangtan University, Xiangtan 411105, China*

[*]*Corresponding author: xiaosiguo@xtu.edu.cn*

Received September 24, 2013; accepted November 5, 2013; posted online December 9, 2013

$Ce^{3+}/Er^{3+}/Bi^{3+}$ triply-doped yttrium aluminum garnet (YAG) is synthesized using co-precipitation method. The Bi^{3+} concentration-dependent near-infrared (NIR) emission behavior is systemically investigated. The NIR emission of Er^{3+} ions at 1531 nm is enhanced threefold by the addition of 7 mol% Bi^{3+}. Bi^{3+}doping results in the formation of exciton in YAG and the variation in the local environment of the doped rare-earth ions. The enhancement in NIR luminescence is ascribed to the combined effects of the sensitization of exciton→Ce^{3+} →Er^{3+} and the Bi^{3+} doping-induced adjustment of the local environment for Ce^{3+} and Er^{3+} ions.

OCIS codes: 260.0260, 260.2160, 260.3800.
doi: 10.3788/COL201311.122602.

Near-infrared (NIR) Er^{3+}emission at approximately 1530 nm on its $^4I_{13/2} \rightarrow {}^4I_{15/2}$ transition has attracted attention because of its important applications in fiber amplifiers, solid-state lasers, telecommunications, remote sensing, molecular-based imaging, etc.[1−5]. However, Er^{3+} ions in inorganic matrice show no strong absorption bands in the visible and NIR spectral ranges because of the nature of the $4f$ forbidden transitions. Thus, co-doping the matrix with corresponding sensitizers is necessary to enhance the absorption efficiency of Er^{3+} ions. Good sensitizers for Er^{3+} ions in different matrices include Cr^{3+}, Yb^{3+}, and Ce^{3+} ions, which have broad and strong absorption bands in the visible and NIR spectral ranges as well as channels of efficient nonradiative transfer of the electron excitation energy to Er^{3+} acceptor ions[6]. Ce^{3+} ions are advantageous over the other donors because the dipole allows intra configuration of $4f \rightarrow 5d$ transitions of Ce^{3+}, which are involved in the absorption and energy transfer processes, and the strengths of such transitions exceed those of parity forbidden intra configuration transitions by several orders of magnitude[7]. Meanwhile, the branching ratio of $^4I_{11/2} \rightarrow {}^4I_{13/2}$ transition of Er^{3+} can also be improved via the cross-relaxation process $^2F_{5/2}(Ce^{3+}) + {}^4I_{11/2}(Er^{3+}) \rightarrow {}^2F_{7/2}(Ce^{3+}) + {}^4I_{13/2}(Er^{3+})$. The energy transfer between the Ce^{3+} and Er^{3+} ions efficiently increases the population of $^4I_{13/2}$ level and consequently further enhances the 1530-nm emission[1]. The effects of Ce^{3+} doping on NIR Er^{3+}emission in yttrium aluminum garnet (YAG) have been investigated[8−11]. The 1540-nm emission of Er^{3+} in YAG is enhanced by approximately 1000× after the introduction of Ce^{3+}[1].

The NIR emission of Er^{3+} ions may be further enhanced by improving the absorption of Ce^{3+} in Ce^{3+}/Er^{3+} co-doped materials, of which sensitization is still a feasible approach. Enhancing the NIR emission of Er^{3+} is possible if the Ce^{3+} can be sensitized by other suitable sensitizer ions. Bi^{3+} is a good sensitizer to improve the luminous efficiency of several rare-earth ions[12,13]. Red emission of Eu^{3+} can be remarkably improved by Bi^{3+} sensitization under ultraviolet excitation[14−16]. Several studies have also reported on the visible emission (477 nm) of Bi^{3+}-doped YAG caused by the excitons localized near Bi^{3+} ions[17,18]. The emission bands of Bi^{3+} doping-induced excitons are strongly overlapped with the $4f$–$5d$ absorption bands of Ce^{3+} ions with peak at 459 nm, thereby resulting in the efficient energy transfer from excitons to Ce^{3+} ions in the YAG matrix[19].

In this letter, $Ce^{3+}/Er^{3+}/Bi^{3+}$ triply-doped YAG was prepared using a co-precipitation method. The effect of Bi^{3+} co-doping on NIR emissions was systemically investigated.

$Ce^{3+}/Er^{3+}/Bi^{3+}$-doped YAG ($Y_{(2.79-x)}Al_5O_{12}$: $0.06Ce^{3+}$, $0.15Er^{3+}$, xBi^{3+} ($x = 0$, 0.02, 0.07, 0.11)) was prepared using co-precipitation method followed by heat treatment. $Al(NO_3)_3{\cdot}9H_2O$, $YCl_3{\cdot}6H_2O$, $ErCl_3{\cdot}6H_2O$, $Bi(NO_3)_3{\cdot}6H_2O$, and $Ce(NO_3)_3{\cdot}6H_2O$ aqueous solutions were dissolved in properly deionized water according to the designed mole ratio of the sample; the dissolved aqueous solution was marked as solution A. The NH_4HCO_3 aqueous solution was marked as solution B, the mole ratio of which to cations in solution A is 3:1. The concentrations of solutions A and B were 0.2 mol/L. Precipitates were then obtained by slowly dropping solution A into solution B under constant stirring using a glass rod. The precipitates were filtered and washed thrice with distilled water. After drying at 100 °C for 24 h, the precipitates were pre-sintered at 400 °C for 2 h and then sintered at 1500 °C for 6 h.

The structure of the samples were identified by X-ray diffraction (XRD) on a Bruker D8 advance equipment using Cu tube with Kα radiation of 0.15406 nm in the 2θ range of 20°–80°. The microstructure was analyzed using a JSM-6610 scanning electron microscope (SEM).

The excitation and emission spectra excited by a 469-nm laser were recorded using a FLS-920 spectrofluorimeter (Edinburgh Instruments, UK). All experiments were performed at room temperature.

The XRD patterns of YAG and YAG:$Ce^{3+}/Er^{3+}/xBi^{3+}$ (x = 0, 0.02, 0.07, 0.11) are shown in Fig. 1. All XRD peaks of the samples are consistent with the standard values for the highly crystalline YAG (JCPDS No.79-1891). The results suggest that the structure of YAG ceramics is not altered by the presence of Ce^{3+}, Er^{3+}, and Bi^{3+}. The Bi^{3+} ion is completely embedded into the crystal lattice of YAG by replacing the lattice site of the Y^{3+} ion. The cell parameters of the samples are calculated using the XRD data (inset of Fig. 1). Slight differences are found in the cell parameters among the samples with different concentrations of Bi^{3+} because of the small differences in the ionic radii between the Bi^{3+} and Y^{3+} ions.

The microstructure of the samples with different Bi^{3+} concentrations is shown in Fig. 2. For the sample without Bi^{3+} doping, sphere-like particles with an average size of 2 μm are observed. When 2 mol% Bi^{3+} ions are introduced, most of the sphere-like particles agglomerate and form stick-shaped particles. Agglomeration also increases with further increase in Bi^{3+} concentration. This phenomenon indicates that the introduction of Bi^{3+} ions reduce the eutectic melting point, thereby promoting the aggregation of particles and crystal growth.

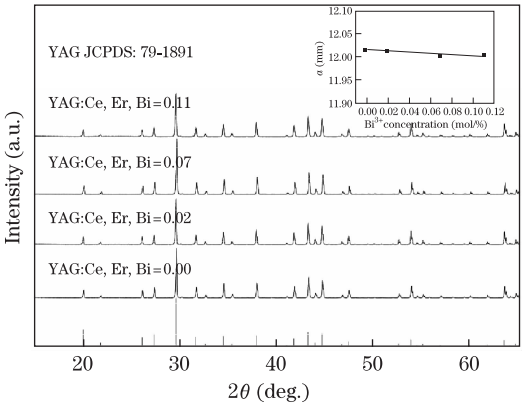

Fig. 1. XRD patterns of YAG, and YAG:$0.06Ce^{3+}/0.15Er^{3+}/xBi^{3+}$ (x = 0, 0.02, 0.07, 0.11). Inset shows the Bi^{3+}-concentration dependence of unit cell parameters of the YAG:$0.06Ce^{3+}/0.15Er^{3+}/xBi^{3+}$ sample (x = 0, 0.02, 0.07, 0.11).

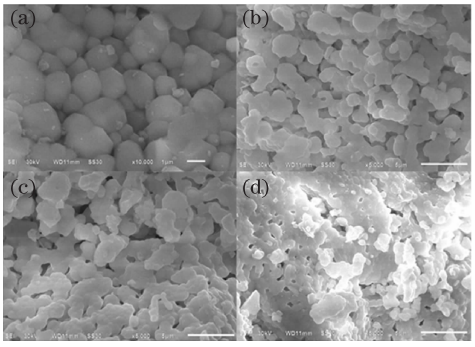

Fig. 2. Scanning electron micrographs of YAG: $Ce^{3+}/Er^{3+}/xBi^{3+}$ with (a) x = 0, (b) 0.02, (c) 0.07, and (d) 0.11.

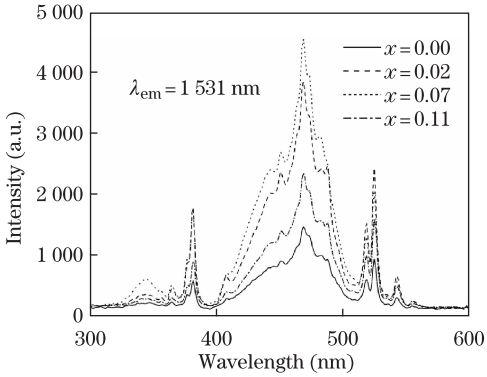

Fig. 3. Excitation spectra of YAG:$0.06Ce^{3+}/0.15Er^{3+}/xBi^{3+}$ (x = 0, 0.02, 0.07, 0.11) under 1531-nm monitoring.

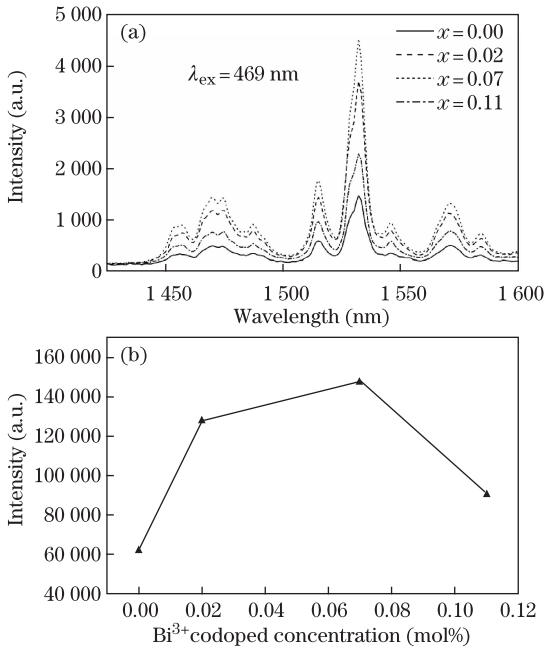

Fig. 4. (a) NIR luminescence spectra of YAG: $0.06Ce^{3+}/0.15Er^{3+}/xBi^{3+}$ (x = 0, 0.02, 0.07, 0.11) under 469 nm excitation. (b) Bi^{3+}-concentration dependence of NIR emission intensity under 469 nm excitation.

The monitored excitation spectra of YAG: $0.06Ce^{3+}/0.15Er^{3+}/xBi^{3+}$ (x = 0, 0.02, 0.07, 0.11) in the 1531-nm emission of Er^{3+} are shown in Fig. 3. Each curve consists of a strong band centered at 469 nm and three relatively weaker peaks at 344, 380, and 525 nm. The different curves were compared, and the results show that the excitation intensity increases gradually with increasing concentration of Bi^{3+} ions from 0 to 7 mol%, and the excitation intensity decreases when the concentration reaches 11 mol%. The obtained NIR region luminescence spectra of YAG:$Ce^{3+}/Er^{3+}/xBi^{3+}$ (x = 0, 0.02, 0.07, 0.11) under 469-nm excitation are shown in Fig. 4(a). NIR emission intensities versus Bi^{3+} concentration is plotted in Fig. 4(b). The luminescence intensity of YAG doped with Er^{3+} and Ce^{3+} ions at 1.5 μm increases gradually with an increase in Bi^{3+} ion concentration from 0 to 7 mol%. However, the luminescence intensity starts to decrease when the concentration of Bi^{3+} exceeds 7 mol%. A threefold increase in NIR luminescence is observed under 469-nm excita-

tion of YAG:$Ce^{3+}/Er^{3+}/xBi^{3+}$($x = 0.07$) compared with YAG:Ce^{3+}/Er^{3+}.

The schematic energy levels with luminescence mechanism of Bi^{3+}, Ce^{3+}, and Er^{3+} ions are shown in Fig. 5. In Ce^{3+}/Er^{3+} co-doped YAG, excitation of Er^{3+} occurs mainly via energy transfer from the $Ce^{3+}-5d$ to the $^4F_{7/2}$ state of Er^{3+} when pumped under 469-nm laser. After excitation of the $Ce^{3+}-5d$ state, the electrons either relax radiatively to the $4f$ ground state, thereby producing broad band luminescence in the visible range, or transfer to the $^4F_{7/2}$ level of Er^{3+}[2,6]. Electrons at $^4F_{7/2}$ level of Er^{3+} ions experience fast nonradiative decay to the $^4I_{13/2}$ level and then decay to the ground state, thereby emitting at 1531 nm. Moreover, the 1531 nm emission is further enhanced via the cross-relaxation process $^2F_{5/2}(Ce^{3+}) + ^4I_{11/2}(Er^{3+}) \rightarrow ^2F_{7/2}(Ce^{3+}) + ^4I_{13/2}(Er^{3+})$. After doping the Bi^{3+} ion, exciton localized around Bi^{3+} ion is formed. Emission bands related to the exciton emission in YAG:Bi^{3+} strongly overlaps with the $4f$–$5d^2$ absorption bands of Ce^{3+} ions peaked at 469 nm[19]. Therefore, the energy transfer from excitons to Ce^{3+} results in enhanced absorption of Ce^{3+}. Correspondingly, the NIR emission of Er^{3+} is further improved.

To verify the sensitization caused by the Bi^{3+}-induced exciton, the excitation spectra of YAG:Ce^{3+}/Er^{3+} and YAG:$Ce^{3+}/Er^{3+}/Bi^{3+}$ monitored at 590 nm were measured (Fig. 6). An increase in excitation intensity is observed for the YAG:$Ce^{3+}/Er^{3+}/Bi^{3+}$. No emission at 590 nm is found in YAG:Er^{3+} in terms of the energy level of Er^{3+} ions. However, 590 nm locates within the range of broad emission band of Ce^{3+}. Therefore, the increased excitation intensity monitored at 590 nm for the YAG:$Ce^{3+}/Er^{3+}/Bi^{3+}$ sample demonstrates the effective energy transfer from excitons to Ce^{3+} ions.

To explore further the mechanism underlying the enhancement of the NIR luminescence, structural variations induced by Bi^{3+} ions are also detected using Eu^{3+} as probe. The emission spectra of YAG:Eu^{3+}(2 mol%) and YAG:Eu^{3+} (2 mol%) co-doped with 2 mol% Bi^{3+} ions under 398-nm excitation are shown in Fig. 7. The emission spectrum mainly consists of a sharp peak at

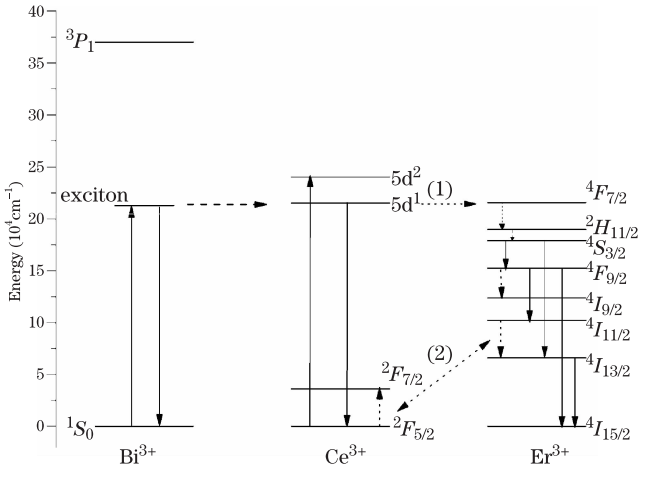

Fig. 5. Schematic energy level diagram of Bi^{3+}, Ce^{3+}, and Er^{3+} ions with transitions and energy transfers that occur in YAG:$Ce^{3+}/Er^{3+}/Bi^{3+}$.

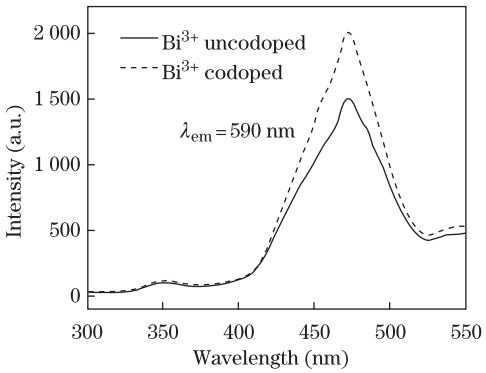

Fig. 6. Excitation spectra of YAG:$Ce^{3+}/Er^{3+}/Bi^{3+}$ and YAG:Ce^{3+}/Er^{3+} monitored at 590 nm.

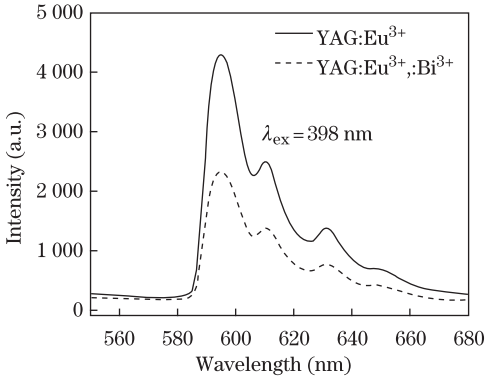

Fig. 7. Emission spectra of YAG:Eu^{3+}(2 mol%) and YAG:Eu^{3+}(2 mol%) co-doped with 2 mol% Bi^{3+} ions under 398-nm excitation.

approximately 590 nm along with a weak peak at approximately 612 nm. The peak at approximately 590 nm is characteristic of $^5D_0 \rightarrow ^7F_1$ transition and that at approximately 612 nm is characteristic of $^5D_0 \rightarrow ^7F_2$ transition of Eu^{3+} ions.

The $^5D_0 \rightarrow ^7F_2$ transition of Eu^{3+} ion is the hypersensitive electronic dipole transition, which is markedly affected by the coordination environment, whereas the $^5D_0 \rightarrow ^7F_1$ transition is the magnetic dipole transition, which is much less sensitive to the coordination environment[20–23]. The magnetic dipole transition is maintained even at low-symmetry environment. Therefore, the relative intensity ratio R, which is defined as $I(^5D_0 \rightarrow ^7F_2)/I(^5D_0 \rightarrow ^7F_1)$, reflects the local environment of Eu^{3+} ion in lattice.

The carefully calculated values for R are given in Table 1. The values of R in YAG:Eu^{3+}/Bi^{3+} are 1.14 and 1.25, respectively. These results suggest that Bi^{3+} ion decreases the local symmetry of luminescence centers in lattice and enhances the electronic dipole transition intensity. In the triply doped YAG, the local environment of the active Er^{3+} and Ce^{3+} ions changes in the visible range. Moreover, the increased electronic dipole transition probability caused by Bi^{3+} doping also enhances the efficiency of energy transfer between Ce^{3+} and Er^{3+} ions, which includes the process (1) $5d^1(Ce^{3+}) + ^4I_{15/2}(Er^{3+}) \rightarrow ^2F_{5/2}(Ce^{3+}) + ^4F_{7/2}(Er^{3+})$ as well as the cross-relaxation process (2) $^2F_{5/2}(Ce^{3+}) + ^4I_{11/2}(Er^{3+}) \rightarrow ^2F_{7/2}(Ce^{3+}) + ^4I_{13/2}(Er^{3+})$. Both the increased Er^{3+} and Ce^{3+} absorption and enhanced energy

Table 1. *R* Value of Eu^{3+} in Eu^{3+}-doped YAG and Eu^{3+}/Bi^{3+} Co-doped YAG under 398-nm Excitation

Bi^{3+} Ion Doping Concentration (mol%)	$R = I(^5D_0 \rightarrow ^7F_2)/I(^5D_0 \rightarrow ^7F_1)$
0	1.14
2	1.25

transfer between Ce^{3+} and Er^{3+} ions are beneficial to the NIR emission of Er^{3+}.

Thus, two factors might enhance the NIR luminescence intensity with the introduction of Bi^{3+} ions. First, the sensitization of excitons to Ce^{3+} ions can improve the excitation efficiency because of the good spectral overlap between the fluorescence bands of excitons and the absorption bands of the acceptor Ce^{3+} ions in the YAG matrix. Second, the change in the local environment of the active ions Er^{3+} and Ce^{3+} ions induced by Bi^{3+} doping enhances the absorption of Er^{3+} and Ce^{3+} ions in the visible range and increases the efficiency of energy transfer between Ce^{3+} and Er^{3+} ions. The combination of these two aspects enhances the NIR emission originating from the $^4I_{13/2} \rightarrow ^4I_{15/2}$ transition of Er^{3+}. This phenomenon proves that Bi^{3+} ion is a good sensitizer and lattice modifier for YAG:Ce^{3+}/Er^{3+} NIR phosphor.

In conclusion, we synthesize pure-phase YAG:$Er^{3+}/Ce^{3+}/Bi^{3+}$ using co-precipitation method. Strong NIR emissions of Er^{3+} ions at approximately 1531 nm are observed under 469-nm excitation. A threefold increase in NIR luminescence is observed because of the addition of Bi^{3+} ions. This phenomenon is due to the sensitization of Bi^{3+} doping-induced excitons to Ce^{3+} ions and the variation in the local environment of the Ce^{3+} and Er^{3+} ions in YAG matrix. The results show that the Bi^{3+} ions can act as sensitizer and lattice modifier for YAG:Ce^{3+}/Er^{3+} to improve its NIR emission.

This work was supported by the National Natural Science Foundation of China (Nos. 61233010 and 51372214), the Hunan Provincial Natural Science Foundation of China (No. 12JJ3063), and the Open Project of State Key Laboratory of Rare Earth Resources Utilization, Changchun Institute of Applied Chemistry, Chinese Academy of Science (No. RERU2013017).

References

1. J. Meng, K. W. Cheah, Z. Shi, and J. Li, Appl. Phys. Lett. **91,**151107 (2007).
2. V. G. Babajanyan, R. B. Kostanyan, and P. H. Muzhikyan, J. Phys. **350,** 012024 (2012).
3. L. H. Slooff, A. Van Blaaderen, A. Polman, G. A. Hebbink, S. I. Klink, F. C. J. M. van Veggel, D. N. Reinhoudt, and J. W. Hofstraat, J. Appl. Phys. **91,** 3955 (2002).
4. Q. Wang, L. Su, H. Li, L.Zheng, X. Xu, H. Tang, X. Guo, D. Jiang, and J. Xu," Phys. Status Solidi A **208,** 2839 (2011).
5. Y. Chen, Y. Lin, H. Zhu, G. Zhang, and Y. Huang, Chin. Opt. Lett. **10,** 021403 (2012).
6. V. G. Babajanyan, R. B. Kostanyan, P. H. Muzhikyan, A. G. Petrosyan, J. Contemp. Phys. **46,** 54 (2011).
7. X. Wang, H. Mao, C. Ma, J. Xu, and X. Zeng, Chin. Opt. Lett. **10,** 071601 (2012).
8. A. L. Denisov, A. F. Umyskov, and I. A. Shcherbakov, Sov. J. Quantum Electron**19,** 167 (1992).
9. Y. Yu, S. Zhang, S. Tie, and M. Song, J. Alloys Comp. **217,** 148 (1995).
10. J. Zhou, Y. Teng, X. Liu, S. Ye, Z. Ma, and J. Qiu, Phys. Chem. Chem. Phys. **12,**13759 (2010).
11. D. Solodovnikov, M. H. Weber, and K. G. Lynn, Appl. Phys. Lett. **93,**104102 (2008).
12. R. Yang, M. Mao, Y. Zhang, Y. Zhuang, K. Zhang, and J. Qiu, J. Non-Cryst. Solids **357,** 2396 (2011).
13. H. S. Yoo, W. B. Im, J. H. Kang, and D. Y. Jeon, Opt. Mater. **31,** 131 (2008).
14. X. Wu, Y. Liang, R. Chen, M. Liu, and Y. Li, J. Mater. Sci. **46,** 5581 (2011).
15. X. T. Wei, Y. H. Chen, X. R. Cheng, M. Yin, and W. Xu, Appl. Phys. B **99,** 763 (2010).
16. M. Li, X. Xiang, W. Yang, W. Li, and L. Kong, J. Inorg. Mater. **24,** 1059 (2009).
17. V. Babin, V. Gorbenko, A. Krasnikov, A. Makhov, E. Mihokova, M. Nikl, S. Zazubovich, and Yu. Zorenko, Phys. Status Solidi B **249,** 1039 (2012).
18. V. Babin, V. Gorbenko, A. Krasnikov, A. Makhov, M. Nikl, S. Zazubovich, and Yu. Zorenko, Radiat. Meas. **45,** 331 (2010).
19. Y. Zorenko, V. Gorbenko, T. Voznyak, M. Nikl, A. Beitlerova, and V. Jary, J. Lumin. **134,** 539 (2013).
20. E. W. J. L. Oomen and A. M. A. van Dongen, J. Non-Cryst. Solids **111,** 205 (1989).
21. S. Basu, D. K. Patel, J. Nuwad, V. Sudarsan, S. N. Jha, D. Bhattacharyya, R. K. Vatsa, and S. K. Kulshreshtha, Chem. Phys. Lett. **84,** 561 (2013).
22. L. Jiang, S. Xiao, X. Yang, J. Ding, and K. Dong, Appl. Phys. B **107,** 479 (2012).
23. M. Shi, H. Li, M. Pan, F. Su, L. Ma, P. Han, and H. Wang, Chin. Opt. Lett. **9,** 051901 (2011).